The Plant Cell, Vol. 21: 2090–2106, July 2009, www.plantcell.org © 2009 American Society of Plant Biologists

Helical Growth of the *Arabidopsis* Mutant *tortifolia2* Does Not Depend on Cell Division Patterns but Involves Handed Twisting of Isolated Cells [W] [OA]

Henrik Buschmann,[a,b] Monika Hauptmann,[a] Dierk Niessing,[c,d] Clive W. Lloyd,[b] and Anton R. Schäffner[a,1]

[a] Institute of Biochemical Plant Pathology, Helmholtz Zentrum München, 85764 Neuherberg, Germany
[b] Department of Cell and Developmental Biology, John Innes Centre, Norwich, NR4 7UH, United Kingdom
[c] Institute of Structural Biology, Helmholtz Zentrum München, 85764 Neuherberg, Germany
[d] Munich Center for Integrated Protein Science at the Gene Center of the Ludwig-Maximilians-University, Munich 81377, Germany

Several factors regulate plant organ growth polarity. *tortifolia2* (*tor2*), a right-handed helical growth mutant, has a conservative replacement of Arg-2 with Lys in the α-tubulin 4 protein. Based on a published high-resolution (2.89 Å) tubulin structure, we predict that Arg-2 of α-tubulin forms hydrogen bonds with the GTPase domain of β-tubulin, and structural modeling suggests that these contacts are interrupted in *tor2*. Consistent with this, we found that microtubule dynamicity is reduced in the *tor2* background. We investigated the developmental origin of the helical growth phenotype using *tor2*. One hypothesis predicts that cell division patterns cause helical organ growth in *Arabidopsis thaliana* mutants. However, cell division patterns of *tor2* root tips appear normal. Experimental uncoupling of cell division and expansion suggests that helical organ growth is based on cell elongation defects only. Another hypothesis is that twisting is due to inequalities in expansion of epidermal and cortical tissues. However, freely growing leaf trichomes of *tor2* mutants show right-handed twisting and cortical microtubules form left-handed helices as early as the unbranched stage of trichome development. Trichome twisting is inverted in double mutants with *tor3*, a left-handed mutant. Single *tor2* suspension cells also exhibit handed twisting. Thus, twisting of *tor2* mutant organs appears to be a higher-order expression of the helical expansion of individual cells.

INTRODUCTION

As a result of cell division and cell elongation, plant organs expand into space to generate the growth axis. That axis may be straight but in some cases can be composed of cell files that are not aligned in parallel but are twisted around the axis. Expression of this feature during organ expansion is called helical growth. In *Arabidopsis thaliana*, helical growth can be induced by mutation. Indeed, the analysis of helical growth mutants has proved to be especially informative concerning the relationship between microtubule behavior and the direction of organ growth (for review, see Ishida et al., 2007a). The molecular identification of mutant loci has revealed mutations in α- and β-tubulin (Thitamadee et al., 2002; Ishida et al., 2007b) as well as in several microtubule-associated proteins from plants (Whittington et al., 2001; Buschmann et al., 2004; Nakajima et al., 2004; Sedbrook et al., 2004; Shoji et al., 2004; Kaloriti et al., 2007; Perrin et al., 2007; Nakamura and Hashimoto, 2009). When applied in moderate concentrations, microtubule drugs also result in helical organ torsions (Furutani et al., 2000). Depending on the allele, helical growth mutants show either left-handed or right-handed organ torsions. Interestingly, although exceptions have been reported (Furutani et al., 2000; Thitamadee et al., 2002; Yuen et al., 2003), left-handed growth is usually epistatic over right-handed growth.

There is a long-standing paradigm that, during rapid cell growth, microtubules direct the alignment of cellulose microfibrils (for a discussion of models, see Baskin, 2001, 2005). In many cases, microtubules and microfibrils encircle the cell perpendicular to the direction of cell expansion, and it is thought that microfibril orientation determines the polarity of cell expansion. Recent analysis of a fluorescence-tagged cellulose synthase has confirmed that this enzyme travels along the tracks provided by microtubules, supporting the idea that microtubules serve as a cytoplasmic template for microfibril orientation (Paredez et al., 2006). Apart from this interphase function in cell wall assembly, microtubules play important roles during mitosis and cytokinesis where they are involved in the regulation of tissue patterning and organ shape (Jürgens, 2005; Lloyd and Buschmann, 2007; Müller et al., 2009).

Two opposing models may explain the development of a helical growth phenotype in *Arabidopsis* organs. According to the model by Hashimoto and coworkers (Furutani et al., 2000; Hashimoto, 2002), organ twisting is based on differences in cell elongation between epidermal cells and the underlying cortical

[1] Address correspondence to schaeffner@helmholtz-muenchen.de.
The author responsible for distribution of materials integral to the findings presented in this article in accordance with the policy described in the Instructions for Authors (www.plantcell.org) is: Anton R. Schäffner (schaeffner@helmholtz-muenchen.de).
[W] Online version contains Web-only data.
[OA] Open access articles can be viewed online without a subscription.
www.plantcell.org/cgi/doi/10.1105/tpc.108.061242

cells. The epidermal cells of both *Arabidopsis* mutants or wild-type plants treated with microtubule-targeting drugs grew in helical files, and the cortical cells were often found to be swollen and impaired in longitudinal expansion. The cortical microtubules of epidermal cells were arranged in an oblique (rather than a strictly transverse) fashion, therefore shifting the axis of growth anisotropy to an oblique angle. As a result of the discrepancy in expansion between the two tissues, epidermal cells are assumed to tilt over to produce a rotation of the distal part of the organ.

Another model for helical organ growth can be derived from the cell division patterns in meristems. Helical patterns of division in a ring of initial cells give rise to the root epidermis and lateral root cap (Baum and Rost, 1996), and it is conceivable that these helical division patterns could impact on organ expansion and therefore organ shape. Interestingly, the twisting mutants *lopped1/tornado1* and *tornado2* show a number of defects in root meristem organization (Cnops et al., 2000). Based on this observation, Wasteneys and Collings (2004) speculated that helical growth could be based on an interference with the stereotypical division patterns in meristems.

Microtubules are deeply involved in the helical growth phenomenon (Lloyd and Chan, 2002). Microtubules are polymers consisting of 13 files of tubulin arranged to form a hollow cylinder (Löwe et al., 2001). Since tubulin is mainly added at the microtubule plus end, but is lost at the minus end, microtubules exhibit treadmilling (Shaw et al., 2003). Tubulin dimers are added head to tail onto microtubules so that the exposed fast-growing plus end is crowned by β-tubulin subunits (Nogales et al., 1999). Tubulin itself is a heterodimer made from α- and β-tubulin subunits and has GTPase function. The docking of an arriving tubulin dimer is assumed to trigger GTPase function in the β-tubulin subunit of the previous dimer. This induces a conformational switch in tubulin, which appears to alter its capacity to support the tubulin lattice (Buey et al., 2006). Microtubule plus ends exhibiting a GTP cap (i.e., β-tubulin subunits carrying mainly unhydrolyzed GTP) are stable and continue polymerization. However, when the GTP cap is lost, microtubules are likely to undergo depolymerization (catastrophe). The α- and β-tubulin proteins are an outstanding example of evolutionary protein optimization among the eukaryotic kingdoms (McKean et al., 2001; Buschmann and Lloyd, 2008). They are important drug and herbicide targets, and mutations leading to hyper- or hyposensitivity have been reported (Anthony et al., 1998; Richards et al., 2000; Morrissette et al., 2004). In yeast, tubulins impaired in GTPase function were reported to result in hyperstabilized microtubules (Anders and Botstein, 2001). A collection of plant tubulin mutations assumed to impact on microtubule stability was reported for plants. However, high-resolution structural insight allowing a mechanistic interpretation was not employed (Ishida et al., 2007b).

In this article, we present the helical growth mutant *tortifolia2* (*tor2*), named after the helical growth mutant prototype *tortifolia*, described by Reinholz (Reinholz, 1947; Buschmann et al., 2004). The phenotype of this mutant is based on a conservative amino acid exchange of the Arg-2 residue of α-tubulin 4. We significantly improved earlier modeling of mutations in α-tubulin (Ishida et al., 2007b) by employing a higher-resolution crystallographic structure (at 2.89 Å; Nettles et al., 2004) and inspecting the original electron density map. This allowed us to predict hydrogen bonds between residues and to assess the potential effect of the *tor2* mutation.

Our analysis suggests that the Arg-2 residue of α-tubulin interacts via hydrogen bonds with the GTPase region of β-tubulin and that the Lys residue found in the *tor2* mutant does not form these bonds. In accordance with this prediction, we find that several microtubule dynamic instability parameters are significantly altered in the *tor2* background. The *tor2* mutation produces right-handed helical growth in various organs and has a major impact on epidermal cell form. We rule out the possibility that division patterns are involved in helical growth by manipulating the direction of organ twisting in hypocotyls that only undergo interphase cell elongation. Furthermore, by presenting examples of helical growth for *Arabidopsis* cells growing in isolation, we show that torsion is inherent within the single cell and is not necessarily an expression of tissue interactions. We discuss these findings in relation to models for helical cell and organ growth.

RESULTS

Arabidopsis plants with helically twisted leaf petioles were isolated in a screen for mutants impaired in leaf development. In addition to the formerly identified *tor1* mutant (Fabri and Schäffner, 1994; Buschmann et al., 2004), two further complementation groups were found and termed *tor2* and *tor3*. *tor2* and *tor3* mutants show right-handed and left-handed petiole torsions, respectively. This article focuses on the analysis of the *tor2* mutant but employs the *tor3* mutant to resolve a specific question.

The *tor2* Phenotype Is Caused by a Missense Mutation in α-Tubulin 4

Fine mapping of the semidominant *tor2* locus identified its position in the top region of chromosome 1. Sequencing of the α-tubulin 4 candidate gene (At1g04820) in this region revealed a G-to-A transition for the fifth nucleotide of its open reading frame. This mutation results in a conservative exchange of the second amino acid Arg (R) with Lys (K). The R2 residue of α-tubulin is highly conserved and can be found in several hundred GenBank entries for α-tubulin. We next confirmed that the R2K mutation of α-tubulin 4 is responsible for the *tor2* phenotype (Figures 1A and 1B). A T-DNA insertion mutant of the α-tubulin 4 gene was identified in the SALK collection. RT-PCR analysis of a homozygous line confirmed the knockout of α-tubulin 4. However, respective plants did not show any obvious phenotype (Figure 1C; see Supplemental Figure 1 online). When wild-type or α-tubulin 4 knockout plants were transformed with a construct carrying the entire α-tubulin 4^{R2K} gene, a typical *tor2* phenotype was generated (Figure 1D). The same plant lines transformed with the wild-type α-tubulin 4 gene did not show any obvious phenotype. These experiments confirm that the *tor2* phenotype results from the expression of the dominant-negative R2K mutation of α-tubulin 4.

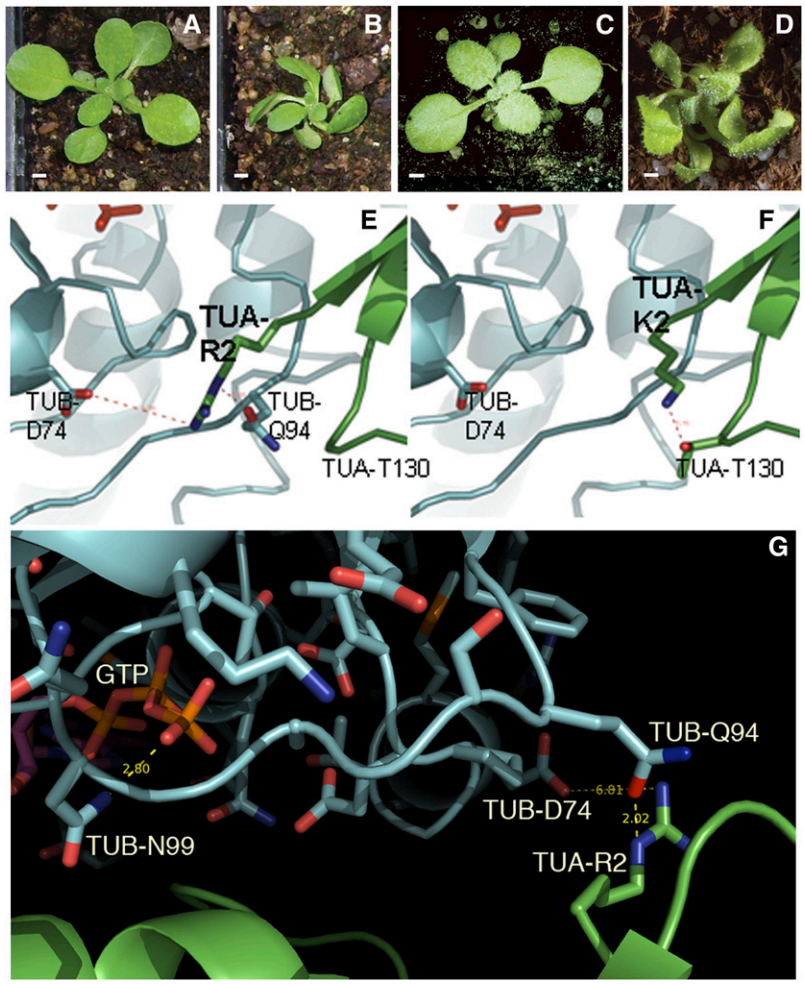

Figure 1. Rosette Phenotype of α-Tubulin 4 Mutants and Structural Models of Wild-Type and Mutant α-Tubulin.

(A) L*er* wild type.
(B) *tor2* (L*er* background).
(C) *tua4* knockout (Col background).
(D) *tua4*^{R2K} expression in *tua4* knockout plants.
(E) Interactions of wild-type TUA-R2 with TUB-D74 (distance 5.6 Å), TUB-Q94 (distance 2.6 Å), and TUA-T130 (distance 4.9 Å).
(F) The mutant isoform TUA-K2 is modeled to interact with TUA-T130 (distance 2.9 Å) only. The predicted distance of TUA-K2 to TUB-D74 is larger than 10 Å.
(G) Overview of this region for wild-type α-tubulin shows the proximity to the GTP nucleotide in TUB. β-Tubulin (TUB), blue backbone; α-tubulin (TUA), green backbone. Small yellow numbers indicate distances along the yellow lines in Å.
Images were prepared with coordinates from published structures (PDB-ID: 1TVK) (Nettles et al., 2004). Bars = 1 mm in **(A)** to **(D)**.

The R2K Mutation Is Predicted to Interrupt Interactions with Residues of the GTPase Switch of β-Tubulin

To establish the spatial placement and potential interactions of the α-tubulin R2 residue, we employed the published bovine tubulin dimer structure (Löwe et al., 2001). Importantly, all interacting residues are fully conserved in *Arabidopsis* α-tubulin and β-tubulin proteins when compared with this heterologous model. We were able to localize the α-tubulin R2 residue with high confidence and found that it is likely to form interdimer interactions through hydrogen bonds with Q94 and D74 of β-tubulin (of the following tubulin dimer) (Figure 1E). To further confirm this interpretation, we then used the corresponding structure factors of the model with the highest available resolution (2.89 Å, PDB-ID: 1TVK) (Nettles et al., 2004). Electron density showed that the positions of the amino acids and their side chains in the structural model are justified and that α-tubulin R2 and β-tubulin Q94, in particular, are localized with high confidence. The region around β-tubulin D74 was less well defined. Both intermolecular contacts of α-tubulin R2 with the β-tubulin subunit could affect the GTP/GDP binding site of β-tubulin, since D74 and Q94 locate to a region in β-tubulin that corresponds to

the Switch I and Switch II region of classical GTPases (Löwe et al., 2001). Next, we used the structural model to evaluate the potential effect of the α-tubulin R2K mutation. Based on energetically favorable confirmations from rotamer libraries, we found that K2 can be aligned sufficiently close to α-tubulin T130 (2.9 Å distance) and to α-tubulin E3 (2.5 Å; see Supplemental Figure 2 online) to allow stable intramolecular interactions (Figure 1F). By contrast, the intermolecular interactions with Q94 and D74 of β-tubulin appear to be less favored in the α-tubulin mutant R2K. Thus, intramolecular interactions are likely to be strengthened by the R2K mutation, whereas the interdimer contacts are less likely to form and are probably weakened (Figure 1F). Our results are consistent with the possibility that the α-tubulin R2K mutation alters the GTPase activating function of β-tubulin, thereby affecting microtubule assembly (see overview of this region for the wild type in Figure 1G).

Microtubules in *tor2* Show Altered Dynamics

To test the prediction that the α-tubulin 4 R2K mutation affects microtubule dynamic instability, we created $35S_{pro}$:EB1-green fluorescent protein (GFP) and $35S_{pro}$:GFP-TUB6 microtubule marker lines in *tor2* and Landsberg erecta (L*er*) backgrounds. Microtubule dynamics were analyzed in 3-d-old plants germinated on Murashige and Skoog (MS)-based agar plates. The rate of microtubule polymerization was reduced in *tor2* compared with the L*er* reference line. This was true for both EB1-GFP measured in hypocotyls and GFP-TUB6 measured in cotyledon epidermal cells (Figure 2A). We found that the rate of microtubule depolymerization was also reduced in *tor2*. Plus end catastrophe and lagging end shrinkage were significantly slower in *tor2* than in the L*er* background (Figures 2B and 2C). Based on the Student's *t* test, the difference between *tor2* and L*er* polymer growth and shrinkage rates were statistically significant for all measurements (Figures 2A to 2C). When compared with L*er*, leading ends of *tor2* microtubules spent less time polymerizing but spent an increased amount of time in a paused state and in shrinkage (Figure 2D). Consistently, microtubule dynamicity was significantly reduced in *tor2* (Figure 2E). Catastrophe and rescue frequencies, calculated over the entire lifetime of randomly selected microtubules, were significantly increased in *tor2* compared with L*er* (Figure 2E). This was also evident from kymographs, where L*er* often showed leading end polymerization throughout the entire period of observation (4 min). By contrast, *tor2* microtubules showed a hesitant forward and backward movement (Figure 2F). Indeed, a difference in L*er* and *tor2* microtubule behavior can be readily observed in accelerated movies (see Supplemental Movie 1 online). We next asked whether these defects in *tor2* microtubule dynamics would impact the number of microtubules or microtubule bundles present in the cortical array. Microtubule density does not, however, seem to be significantly altered in *tor2* when compared with L*er* (see Supplemental Figure 3 online). Instead, the *tor2* defect appears to affect the length of the EB1 comets at the microtubule plus end. Visual comparison suggests only a slight difference between EB1 comet size in *tor2* and L*er* (see Supplemental Figure 4 online); however, when we quantified the fluorescence distribution along normalized EB1-GFP comets, we found that the tail of *tor2* EB1 comets is significantly more fluorescent (Figure 2G). This suggests that *tor2* plus end comets are longer.

The *tor2* Mutation Renders Root Elongation Hypersensitive to Microtubule Drugs

We next asked whether *tor2* responds differentially to drugs affecting microtubule stability. Root length of mutant and wild-type plants germinated on agar plates containing microtubule drugs was measured (Figure 3). We found that *tor2* root elongation was hypersensitive to the microtubule destabilizing drugs oryzalin and propyzamide. However, elongation of *tor2* roots was also slightly hypersensitive to the microtubule stabilizing drug taxol. The more sensitive response to the drug application was statistically significant for at least two concentrations in all cases (Figure 3). All experiments were repeated and yielded the same trend.

Right-Handed Helical Growth of *tor2* May Be Based on a Genetic Pathway Independent from tor1

Young *tor2* leaves show straight leaf petioles similar to those of the wild type. However, during expansion growth, petioles start to twist, leading to a right-handed rotation of the lamina with an average speed of 24° per day (calculated for days 13 to 21) (Figure 4A). To investigate whether *tor2* was affected in the same genetic pathways as the right-handed *tor1* (*spr2*) mutant, homozygous double mutants were bred. *TOR1* encodes a plant-specific microtubule-associated protein that functions in orienting cortical microtubules (Buschmann et al., 2004; Shoji et al., 2004). The *tor1 tor2* double mutant clearly shows an additive leaf twisting phenotype. The twisting of *tor1 tor2* double mutant leaves was faster (49° per day) than that of the *tor1* and *tor2* single mutants, and the final extent of leaf rotation was more pronounced (Figure 4B). In *tor1 tor2* double mutant plants, we frequently observed leaf rotations larger than a full turn, demonstrating the developmental plasticity of the process (Figure 4C).

Because these results suggested that *tor2* constitutes a right-handed helical growth pathway independent from *tor1*, we analyzed its phenotype in more detail. Apart from leaf petioles, right-handed growth was seen in roots, hypocotyls, stems, and flowering organs of *tor2* (Figures 4 and 5; see Supplemental Figure 5 online), and this was combined with a general dwarfing of plant stature (Figure 4D; see Supplemental Figure 6 online). The *tor2* mutation has a particularly strong impact on epidermal cell growth. In roots, soon after cell file twisting becomes apparent, epidermal cells start to swell and the final cell shape is often spherical (Figures 4E to 4H). In *tor2* hypocotyls, epidermal cells occasionally resume a new axis of growth leading to cone-like protrusions (see Supplemental Figure 6 online). In plants, microtubules have several functions during cell division. To detect a possible defect in chromosome segregation and/or cytokinesis in *tor2*, we analyzed the DNA content of *tor2* mutant cells by flow cytometry. However, flow cytometry of nuclei from rosette leaves and excised shoot meristems did not show a significantly altered pattern of DNA content compared with the wild type (see Supplemental Figure 7 online). Thus, the α-tubulin 4 mutation observed in *tor2* has no observable effect on the segregation of chromatin.

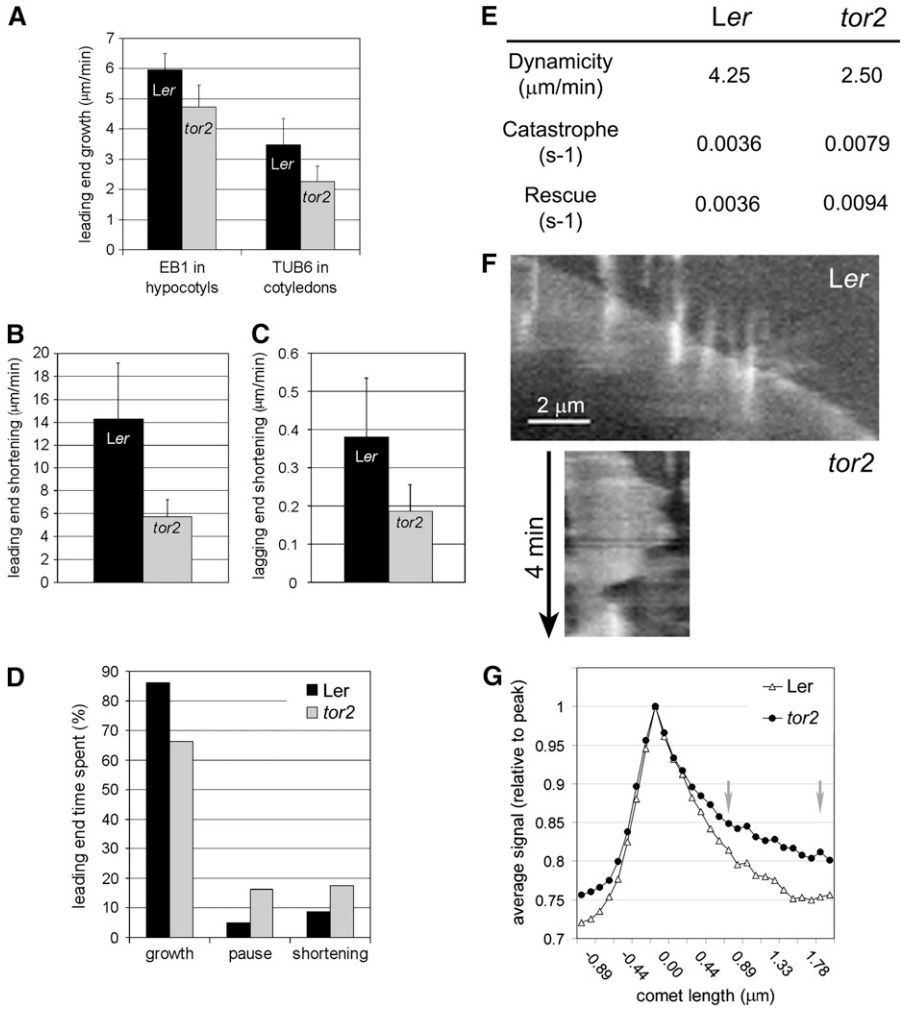

Figure 2. Microtubule Dynamics Are Dramatically Altered in *tor2* Background.

(A) Microtubule polymerization was assessed by measuring the speed of leading (plus) end growth using GFP markers EB1 and TUB6. Irrespective of the marker or the tissue type, *tor2* plus end growth was significantly slower (*t* test, $P < 0.05$).

(B) Microtubule depolymerization at the plus end was assessed by measuring shortening during catastrophe in cotyledon cells. *tor2* microtubules show significantly slower catastrophes (*t* test, $P < 0.05$).

(C) Additionally, microtubule depolymerization was assessed by measuring the speed of lagging end (minus end) shortening in cotyledon cells. The *t* test suggested a significantly slower rate of depolymerization ($P < 0.05$). Each value (±SD) presented in **(A)** to **(C)** is based on $n \geq 40$ microtubules.

(D) Based on randomly selected microtubules, we measured the life history (percentage of time spent) of the leading end of wild-type and *tor2* microtubules in cotyledon cells. *tor2* spends more time in pause and shrinkage when compared with the wild type.

(E) Based on randomly selected microtubules, we measured microtubule dynamicity and the frequency of catastrophe and rescue. These analyses were performed in cotyledon cells, since they contain less crowded and less bundled microtubule arrays than hypocotyls or roots, allowing far more accurate measurements. Leading end dynamicity (cumulative forward and backward movement of the plus end, unit = μm/min) is dramatically altered in *tor2*. Catastrophe and rescue frequencies were calculated in relation to total time spent. In *tor2*, both catastrophe and rescue were significantly more frequent. L*er* = 5256 s observation time; *tor2* = 6728 s observation time.

(F) Kymographs recording the leading end using GFP-TUB6 in cotyledon cells for 4 min each. Wild-type microtubules (L*er*) often showed prolonged periods of polymerization, whereas microtubules in *tor2* behaved erratically and frequently switched between pause, polymerization, and depolymerization.

(G) Plus end comets of *tor2* dim less quickly than those of the wild type. Fluorescence intensity of comets was measured using images of EB1-GFP in hypocotyl cells. The maximum signal was set to one and given the position zero. $n = 25$ comets for both L*er* and *tor2*. The fluorescence values at the points between the two arrows are statistically different for L*er* and *tor2* ($P < 0.05$).

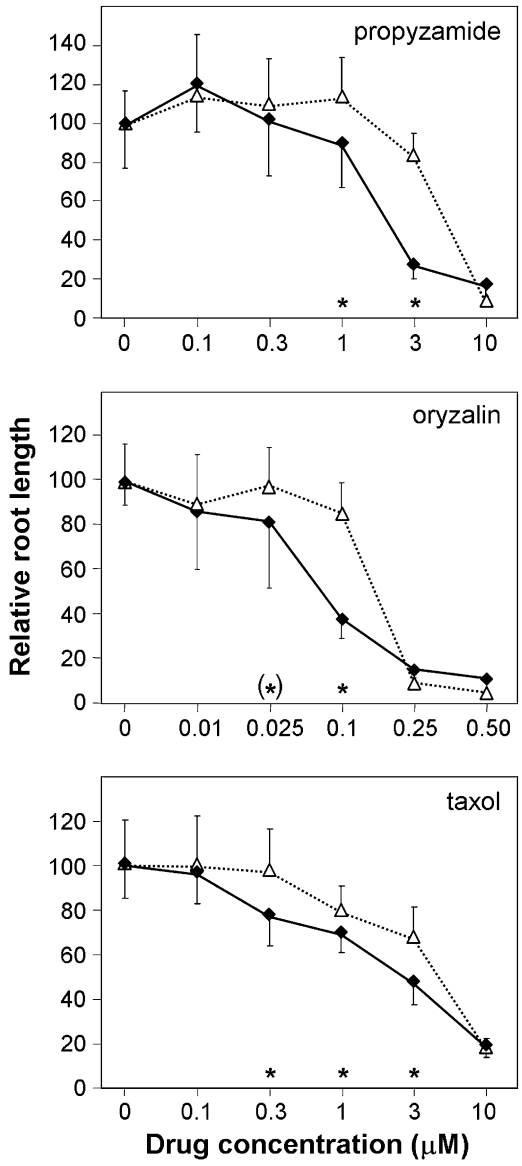

Figure 3. Sensitivity of Root Elongation to Microtubule-Targeting Drugs.

Seedlings were grown for 8 d on agar plates supplemented with 0 to 10 μM propyzamide, 0 to 0.50 μM oryzalin, and 0 to 10 μM taxol as indicated (see Methods). Relative lengths of primary roots of the wild type (triangles, dotted lines) and *tor2* (rhombs) measured using Image J software (n = 13 to 35, ±SD) are displayed; wild-type control roots were approximately twice as long as *tor2* control roots. Statistical tests based on the normally distributed values indicate that hypersensitivity of *tor2* is significant in the critical regions of concentration in all three cases as indicated by asterisks (P values < 0.005 and <0.02 for asterisks in brackets).

Helical Organ Growth Induced by Drugs or the *tor2* Mutation Are Not Caused by Effects on Cell Division

The *Arabidopsis* root meristem exhibits a ring of initial cells that generates the epidermis and peripheral root cap (Baum and Rost, 1996). These T-junctions, where the founder cell splits longitudinally to generate two cell files, arise on a rising spiral around the apical meristem. In longitudinal sections of root tips, the staggered position of these T-junctions is indicative of the spiral division pattern by which they were generated. We therefore asked whether this pattern of T-junctions can be identified in root tips of *tor2* and whether it is altered in this mutant. Staining of roots with propidium iodide and imaging with a confocal microscope readily revealed the T-junctions (Figures 5A and 5B). In wild-type and *tor2* roots, T-junctions were present in a staggered manner consistent with a spiral pattern of cell division in the ring of initials. To assess a possible effect on organ growth, we counted the number of cells between the first and second T-junction for the wild type and *tor2*, corresponding to the steepness of the helix produced. However, no significant difference between *tor2* and the wild type was found (*tor2* = 5.3 and wild type = 5.2; n = 13). Although in *tor2* columella cells and the quiescent center occasionally appeared slightly misshapen, no obvious effect on tissue patterning was detected.

To conclusively rule out the possibility that aberrant cell division patterns produce helical organ growth, we used *Arabidopsis* hypocotyls as a model. Postgermination hypocotyl elongation does not involve significant epidermal or cortical cell divisions (Gendreau et al., 1997; Collett et al., 2000). When grown on MS-based media without drugs, light-grown *tor2* hypocotyls show obvious right-handed growth and wild-type hypocotyls were straight (Figure 5C). Propyzamide (3 μM) produced left-handed helical growth in wild-type hypocotyls, indicating that drug-induced helical growth in wild-type hypocotyls is based on an effect on cell elongation and not cell division. *tor2* hypocotyl growth remained right-handed at this propyzamide concentration. At the highest concentration of 9 μM propyzamide, wild-type hypocotyl growth became somewhat erratic, showing straight, left-handed, and right-handed hypocotyls. However, *tor2* plants growing on 9 μM propyzamide showed an inversion of hypocotyl growth from a right-handed helix to a left-handed helix (Figure 5C). This shows that the direction of *tor2* hypocotyl growth can be overridden from right-handed to left-handed at a late developmental stage, when organ growth solely depends on cell elongation.

Leaf Trichomes of *tor2* Show Right-Handed Twisting and Increased Branching

Since our analyses indicated that helical growth is indeed based on cell elongation, we asked whether the *tor2* mutation has an effect on freely growing cells outside of an organ context. Whereas root hairs of *tor2* appeared largely normal, leaf trichomes had a striking phenotype: *tor2* trichomes were twisted and bent, trichome branches were usually longer than in the wild type, and the average number of branch points was increased (Figures 6A and 6B, Table 1). When viewed from above, the majority of *tor2* trichomes showed branches that bend to the right (Figure 6B). Interestingly, we found that the direction of trichome twisting was inverted in *tor2 tor3* double mutants (Figures 6B and 6D). *tor3* is a novel mutation that produces left-handed helical growth in petioles (see Supplemental Figure 8 online); however, the *tor3* single mutant has no obvious trichome

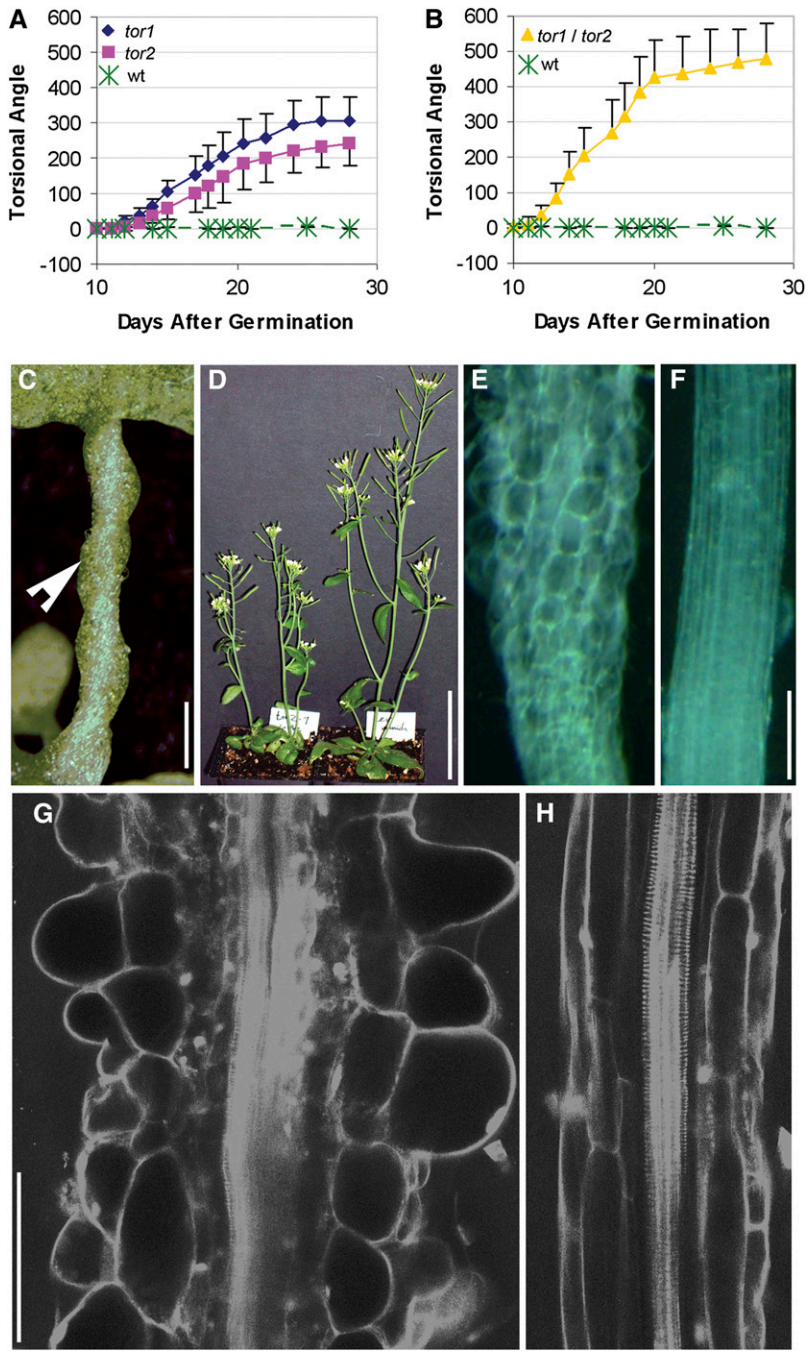

Figure 4. Helical Growth and Epidermal Cell Swelling in *tor2* Mutant Background.

(A) and **(B)** Petiole twisting of *tor* mutants in comparison to the wild type. The position of laminae from primary leaves was monitored during growth and recorded in relation to the horizontal position (set to 0°; 360° is a complete right-handed turn). Note that twisting of the *tor* petioles does not start before plants are 10 d old.

(A) Petiole twisting of single mutants *tor1* and *tor2*.

(B) Petiole torsion of the *tor1 tor2* double mutant is enhanced. The additive phenotype may indicate separate genetic pathways.

(C) Extreme twisting seen in a *tor1 tor2* double mutant petiole. Arrowhead indicates full rotation (360°) of the petiole.

(D) Inflorescence phenotype of *tor2* (two plants shown, left) and wild type (one plant shown, on the right).

(E) Root elongation zone of *tor2*. Cell files of the elongation zone show right-handed twisting. Epidermal cell swelling is seen in close proximity to the onset of twisting.

(F) Wild-type elongation zone.

(G) Confocal z-section of a fully differentiated 6-d-old *tor2* root stained with propidium iodide. Epidermal and cortical cells have a swollen appearance.

(H) Corresponding wild-type root.

Bars = 1 mm in **(C)**, 5 cm in **(D)**, 100 μm in **(E)** and **(F)**, and 75 μm in **(G)** and **(H)**.

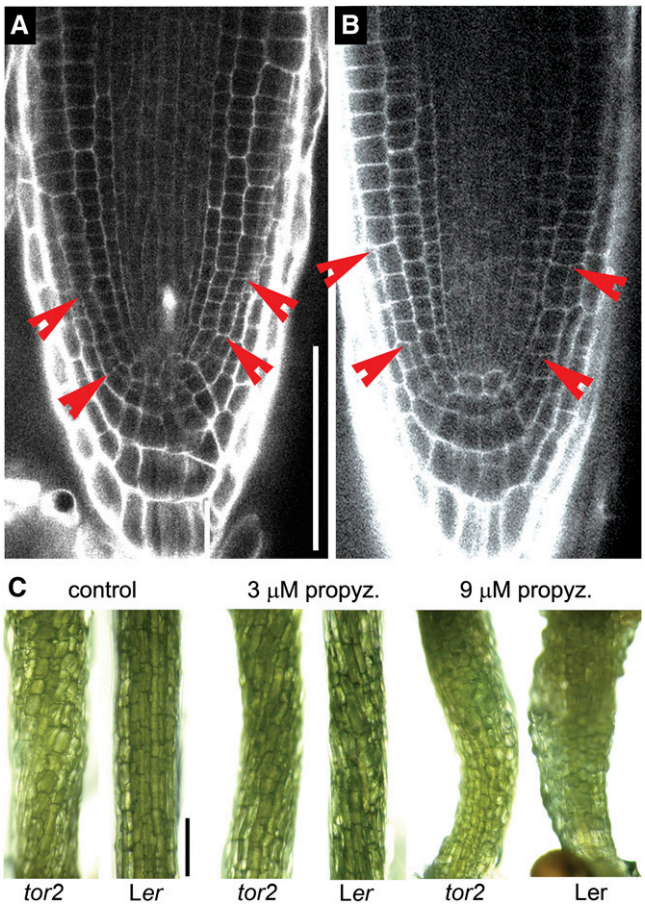

Figure 5. T-Junctions in Roots and Twisted Growth in Hypocotyls.

(A) and **(B)** Root tips of *tor2* and the wild type stained with propidium iodide. Arrowheads point to recently formed T-junctions.

(A) *tor2* root tip.

(B) Wild-type root tip. Note the staggered position of the T-junctions in *tor2* and the wild type. However, shapes of columella and quiescent center cells are somewhat less well defined in *tor2* compared with the wild type.

(C) Hypocotyl growth enables the manipulation of the growth direction independent of effects of cell division. Eleven-day-old *tor2* hypocotyls have a right-handed twist in the absence of drugs, and wild-type hypocotyls are straight. The presence of 3 μM propyzamide has little effect on *tor2*, but wild-type hypocotyls produce a left-handed twist. Propyzamide (9 μM) produces left-handed growth in the *tor2* background.

Bars = 75 μm in **(A)** and **(B)** and 250 μm in **(C)**.

phenotype (Figure 6C). The above observations were confirmed by quantification using a binocular microscope (Table 1). Under the scanning electron microscope, using the papillae (cuticular wax droplets) as landmarks, branches and stalks of *tor2* trichomes showed torsions of consistently right-handed direction, whereas wild-type trichomes were straight only (Figures 6E to 6H). These results show that the right-handed twisting phenotype of *tor2* is expressed in a freely growing cell and does not require tissue-based interactions for it to develop.

zwichel mutants have fewer trichome branches than wild-type plants, and this is combined with a moderate branch elongation defect (Hülskamp et al., 1994; Luo and Oppenheimer, 1999). *ZWICHEL* encodes a calmodulin-regulated kinesin (Oppenheimer et al., 1997; Reddy and Day, 2000). Transient microtubule stabilization using taxol was reported to increase branch initiation in the *zwichel* background (Mathur and Chua, 2000). Overexpression of an N-terminally tagged α-tubulin, which produces right-handed organ torsions in *Arabidopsis*, was reported to mimic the taxol effect on *zwichel* trichomes (Abe and Hashimoto, 2005). We therefore crossed *tor2* into the *zwichel* background. For comparison, we additionally quantified the effects of taxol on *zwichel* single mutants. The *tor2 zwichel* double mutant shows significantly more branch points when compared with the *zwichel* single mutant (Table 1, Figures 6J and 6K). We further confirmed that taxol is capable of producing a second branch point in *zwichel* single mutant trichomes, although with a comparatively low efficiency of 5.5%. In the *tor2 zwichel* double mutant, only a subset of the initiated branches elongated and those that did tended to stay short (Figures 6J and 6K). This suggests that the branch elongation defect seen in *zwichel* mutants was enhanced in the *tor2 zwichel* double mutant background. Indeed, *tor2 zwichel* double mutant trichomes often showed an enhancement of the right-handed twisting seen in the *tor2* background. This was most obvious in unbranched trichomes occasionally seen in *tor2 zwichel* double mutants (Figure 6L).

Left-Handed Cortical Microtubule Arrays in Roots and Trichomes of *tor2*

EB1-GFP lines backcrossed to *tor2* were used to analyze microtubule orientation relative to the cell's axis (Figure 7). In *tor2* roots, epidermal cells of the early elongation zone showed left-handed microtubule arrays, and this was seen before the onset of cell file twisting. Wild-type microtubule arrays of a comparable region were transverse (Figures 7A and 7B). We therefore asked whether freely growing cells like trichomes would also show helical microtubule arrays, focusing on an early stage of trichome development, after the epidermal outgrowth has acquired a cylindrical shape but before branching. Wild-type trichome cells of this stage show cortical microtubule arrays that are denser near the cell's tip compared with the base. However, we routinely observed a spot devoid of microtubules at the apex of the cell. In wild-type trichomes, EB1 comets appeared to encircle the apex, creating a halo of microtubules (see Supplemental Movie 2 online). Interestingly, we found that this cortical array of microtubules was left-handed helical in *tor2* mutants but was mainly transverse in the wild type (Figures 7C and 7D; see Supplemental Movies 2 and 3 online). A quantitative analysis of array orientations based on EB1 movement in movies showed that the majority of *tor2* microtubule arrays in unbranched trichomes was shifted to left-handed positions but was transverse in the wild type (Figure 7E). This demonstrates that the right-handed twisting seen in adult trichomes of *tor2* is preceded by the formation of left-handed cortical microtubule arrays.

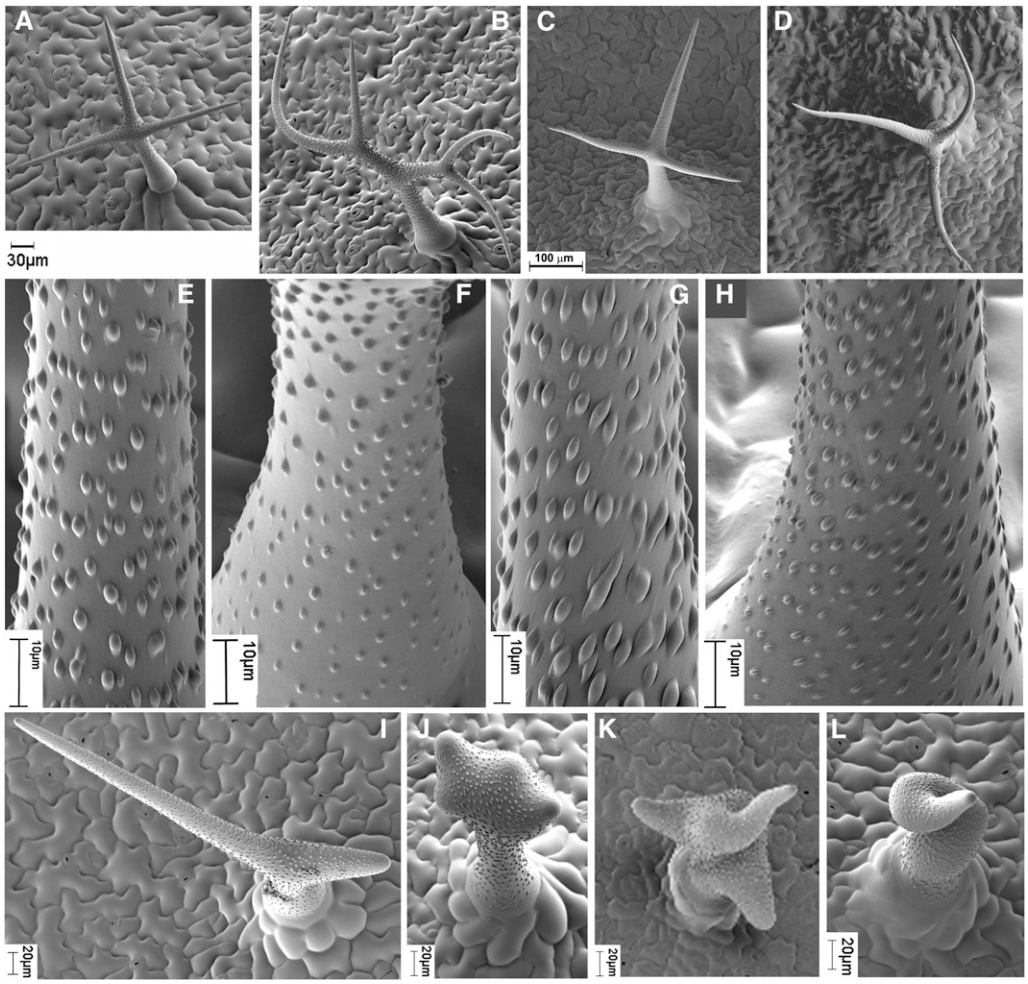

Figure 6. Helical Growth Observed in Trichomes of the *tor2* Mutant Background.

(A) Wild-type trichome.
(B) *tor2* trichome with branches bend to the right. *tor2* mutants have more branch points than wild-type plants.
(C) *tor3* trichomes are straight.
(D) Trichome branches of the *tor2 tor3* double mutant bend to the left.
(E) Close-up of wild-type branch showing cuticular wax droplets.
(F) Wild-type trichome stalk.
(G) Close-up of *tor2* branch showing wax droplets arranged in a right-handed helix.
(H) *tor2* stalk with helically arranged droplets.
(I) *zwichel* trichome showing reduced branching and a branch elongation defect.
(J) to **(L)** Trichome phenotypes seen in *tor2 zwichel* double mutants.
(J) and **(K)** *tor2 zwichel* double mutants show more branch points, but branch elongation is impaired.
(L) *tor2 zwichel* double mutant trichome with exaggerated right-handed twisting.
Bars = 30 μm in **(A)** and **(B)**, 100 μm in **(C)** and **(D)**, 10 μm in **(E)** to **(H)**, and 20 μm in **(I)** to **(L)**.

Cell Suspensions Created from *tor2* Show the Twisting Phenotype

To validate the finding that the *tor2* mutation is capable of producing helical growth in isolated cells, we generated cell suspension cultures from wild-type (L*er*) and *tor2* roots (three lines each). This allowed us to study cell elongation outside the context of a plant organ. Microscopy observation revealed that wild-type lines predominantly formed elongated, cylindrical cells. By contrast, the elongation growth of *tor2* lines was obviously compromised (Figure 8A). In *tor2* lines, we were able to distinguish several characteristic cell-shape classes: elongated cells (data not shown), multipolar cells (top left), rounded cells (bottom left), and helical cells of varying degrees (middle and right). We next quantified the cell shape classes in our suspension lines (Figure 8B). Whereas elongated shapes were predominant in wild-type cells (>70%), this class was diminished

Table 1. Twisting Trichomes and Branch Point Number in *tor2* Mutant Background

	Twisting Direction (%)[a]				Branch Point Number (%)						
Genotype[b]	RH[a]	LH[a]	Straight	Total	0	1	2	3	4	5	Total
L*er* wild-type	0.7	1.3	98	303		2.1	87.1	10.4	0.4		241
tor2	46.3	2.6	51.1	272		6.8	54.4	37.9	1.0		206
tor3	0	1.5	98.5	266			91.8	8.2			171
tor2 tor3	5.4	27.6	67	239		10.3	65.1	23.9	0.7		301
zwi				NA	31.6	68.4					301
zwi (L*er*)[c]				NA	62.2	37.8					516
zwi tor2				NA	45.1	25.2	18.4	9.2	1.9	0.1	727
zwi + taxol				NA	64.2	30.3	5.5				433

NA, not analyzed.

[a]seen from above using a magnifying glass; RH, right-handed; LH, left-handed.

[b]All mutant loci are homozygous.

[c]Homozygous *zwi* lines were generated from a cross against L*er* background in order to compensate for a moderate ecotype-specific effect.

in *tor2* at the expense of (in order of frequency) multipolar, round, and helical cells. Helical cells in *tor2* accounted for >10% and these were predominantly right handed. Thus, helical growth of individual cells was a general capacity of the *tor2* mutant and was not restricted to specialized cell types like trichomes.

DISCUSSION

Helical Organ Growth Is Based on a Cell Elongation Defect

Two opposing models may explain helical organ growth observed in *Arabidopsis* mutants and drug-treated plants. One model predicts that twisting is based on division patterns in meristematic tissues. Cell divisions in the ring of initials that creates the lateral root cap and epidermis occur nonsimultaneously. The pattern of divisions follows a spiral sequence that produces a helical pattern of cell junctions in the apical meristem (Baum and Rost, 1996). It is conceivable that this could impact upon the direction of root growth. Indeed, wild-type root growth shows a subtle bias toward the left-hand direction (Simmons et al., 1995). That helical division patterns could be the basis for helical growth in *Arabidopsis* mutants was also speculated by Wasteneys and Collings (2004). We therefore asked whether the striking twisted growth of *Arabidopsis* helical growth mutants could be based on helical patterns of division in meristems. We were able to identify the staggered T-junctions in the epidermis of both *tor2* and the wild type but could not detect a significant change in the spacing of the T-junctions. Furthermore, we did not observe the patterning defects seen in the *tornado* mutants (Cnops et al., 2000; Figures 5A and 5B).

To gain positive evidence that helical organ growth is based on cell elongation and not cell division, we used postgermination hypocotyl growth as a model. Because hypocotyl growth is largely independent of cell division, it has been used for investigations on cell elongation (Gendreau et al., 1997; Collett et al., 2000). Using hydroxyurea (Pfosser et al., 2007), we confirmed that suppressing cell division did not abolish hypocotyl growth (data not shown). In this study, we further showed that propyzamide is capable of altering the direction of hypocotyl growth in wild-type and *tor2* plants. Taken together, these results suggest that helical growth of wild-type and *tor2* plants is not based on helical division patterns.

Hashimoto and colleagues (Furutani et al., 2000; Hashimoto, 2002) presented an alternative model of helical organ growth according to which, "the driving force for helical growth should come from radial swelling of inner cells" and the "elongating epidermis may function passively just to determine the direction of skewing." Furutani et al. (2000) speculate that cortical microtubules of inner cells have a stronger response to mutation or drug treatment, leading to a severe loss of growth anisotropy, whereas outer cells respond by producing helical microtubule arrays. In this model, epidermal cells are assumed to contain oblique microtubule arrays underneath the load-bearing outer cell wall, and this is thought to result in the deposition of oblique cellulose microfibrils. This is assumed to produce polar cell growth in the direction perpendicular to microtubule and microfibril alignment and, therefore, to helical organ growth (Furutani et al., 2000). The hypothesis of Hashimoto and coworkers is attractive because the majority of helical growth mutants show oblique microtubule arrays in tissues prone to undergo twisting (a few noteworthy exceptions may be found in Sugimoto et al., 2003; Sedbrook, 2004; Ishida et al., 2007a). Our results show that this general tendency holds true for right-handed *tor2*. However, we note that *tor2* shows a dramatic loss of anisotropy in epidermal tissues of roots, and the impact on epidermal cell form may be even more pronounced than the effect on cortical cells (Figure 4G). This contrasts with results obtained for *spiral1* and could mean that the model by Hashimoto and coworkers, where epidermal cells are less affected than cortical cells, may not apply to *tor2* (Furutani et al., 2000). Since *tor2* shows right-handed twisting of cells growing in isolation (Figures 6 and 8), it is tempting to speculate that a somewhat simpler mechanism is responsible for organ twisting in *tor2*: that is, the simultaneous occurrence of cell twisting in different tissues, in the same direction, may lead to a rotation of the entire organ. Evidently, growing organs are capable of integrating the behavior of independent cells into one coherent growth direction.

Handed Cells Elongate in a Helical Fashion

Whereas twisted trichomes have been observed among the *distorted* class of *Arabidopsis* mutants (Feenstra, 1978; Hülskamp et al., 1994; Szymanski et al., 1999), *tor2* is the only mutant

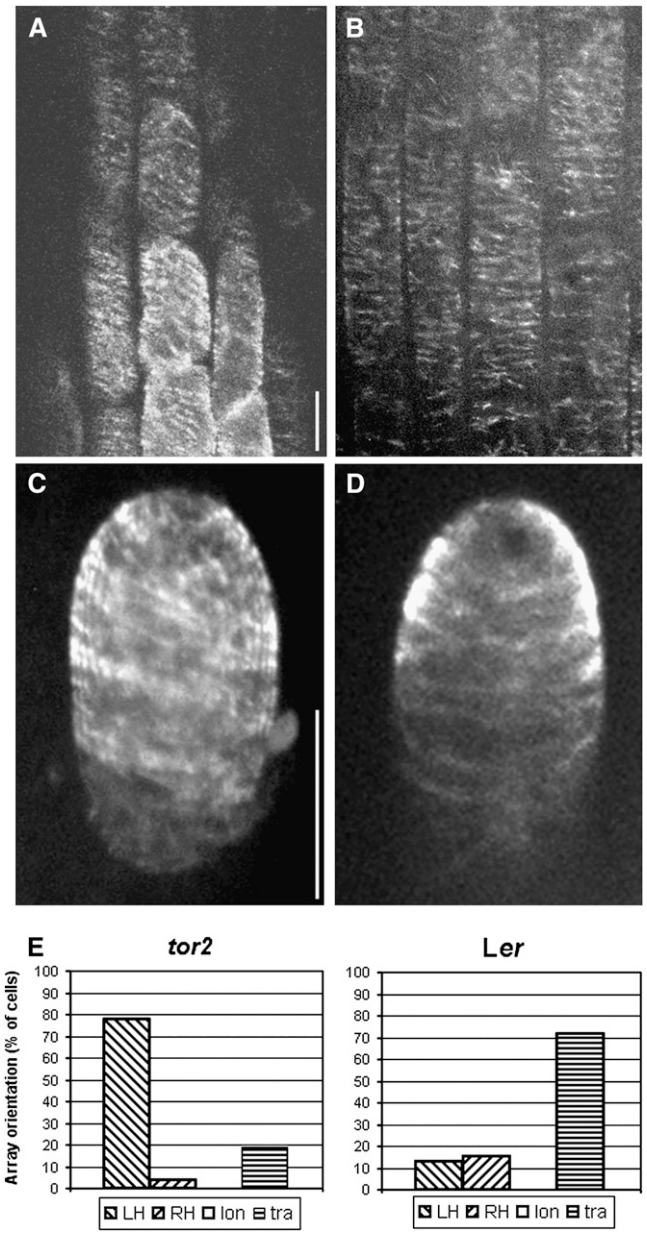

Figure 7. Left-Handed Microtubule Orientations in Roots and Trichomes of *tor2*.

Transgenic lines expressing EB1-GFP were used to highlight cortical microtubules. Bars = 10 μm.

(A) Epidermal cells of the early root elongation zone from *tor2* showed left-handed microtubule arrays, and this was seen before the onset of cell file twisting.

(B) Wild-type arrays in this region were predominantly transverse.

(C) Z/T-projection of EB1 comets seen in unbranched trichomes in the *tor2* background.

(D) Z/T-projection of EB1 comets in the wild type.

(E) Relative frequencies of left-handed (LH), right-handed (RH), longitudinal (lon), and transverse (tra) microtubule arrays in developing trichomes before branching. Only arrays with an inclination >3° from the transverse were considered helical. *tor2*, $n = 27$; wild type, $n = 39$.

reported to show trichome torsions of defined handedness. Although exceptions may eventually be revealed, the identification of genes affected in *distorted*-type trichome mutants has pointed to actin-dependent processes involved in cell elongation. However, some distorted mutants additionally show defects in microtubular organization (e.g., Saedler et al., 2004; Zhang et al., 2005). Our results on the *tor2* mutation of α-tubulin indicate that right-handed trichome twisting is preceded by left-handed microtubule arrays in early trichomes. In *tor2*, helical growth is not limited to trichomes because suspension cells generated from *tor2* mutants also show right-handed cell torsions. It is possible that a closer inspection of other helical growth mutants will show that trichome twisting is a more general feature of this mutant class. The observation that the *tor3* mutation alters

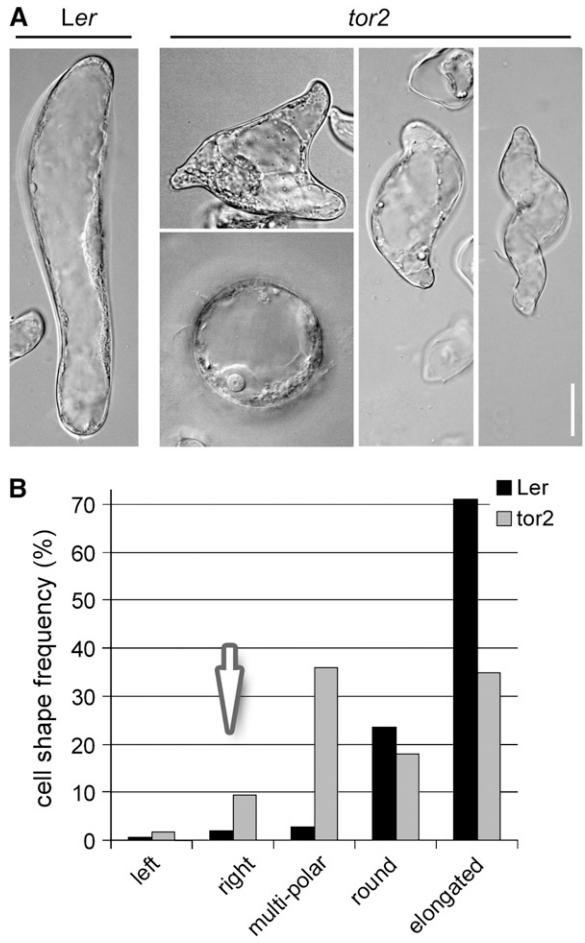

Figure 8. Polarity Defects Seen in Cell Suspensions of *tor2*.

(A) After 1 week of growth in fresh medium, wild-type suspension lines (*Ler*) showed mainly cylindrical shapes, whereas *tor2* suspension cells were usually less elongated and showed multipolar, round, or helical cells. Helical cells in *tor2* varied between spindle-shaped and corkscrew like. Bar = 20 μm.

(B) Quantification of observed cell shape defects. Wild-type, $n = 297$; *tor2*, $n = 278$. In *tor2* suspensions, >10% of cells have helical cell shapes, most of which are right-handed (arrow).

the direction of trichome twisting in *tor2 tor3* double mutants (Table 1, Figure 6) seems to support this notion. The fact that *Arabidopsis tor2* shows helical growth at the single-cell level suggests a mechanistic similarity to other cell types with helical growth (e.g., the *Phycomyces* sporangiophore, the charophyte *Nitella*, and the filamentous algae *Chaetomorpha* and *Cladophora*). These organisms have served as early model organisms to test principles of growth anisotropy in freely growing cells (for review, see Roelofsen, 1965; Preston, 1974). Based on a wide range of experimental approaches, including birefringence analyses and electron microscopy of cell walls, it was concluded that helical growth in these freely elongating cells is based on the handedness exhibited by the helical cell wall texture (Roelofsen, 1951; Frei and Preston, 1961; Probine, 1963).

The Relationship between the Helical Sign of Cell Wall Organization and the Direction of Growth

In all cases, helical growth is thought to occur in a direction perpendicular to the mean alignment of wall microfibrils (Roelofsen, 1965; Hashimoto, 2002; Wasteneys and Collings, 2004; Baskin, 2005). Therefore, the angle of helical growth is a direct translation of the angle of microfibrils in the wall, and Roelofsen (1965) has discussed this in terms of actual values. This means that cells with left-handed wrappings of wall microfibrils should show right-handed growth and vice versa (see Figure 9 for explanation). Some support for this is provided by our observation that the predominantly left-handed cortical microtubules of *tor2* trichomes are accompanied by the opposite right-handed pattern of cuticular wax papillae (Figures 6 and 7). For modeling purposes, the elongation of cells with helically arranged microfibrils has been compared with pulling out a spring (Roelofsen, 1950; Lloyd and Chan, 2002). This showed that certain springs meet the criteria explained above: that is, a line drawn vertically down the spring rotates with the opposite helical sign when the spring is stretched. Helical lamellae of actual plant cell walls are likely to behave differently in detail (shorter microfibrils, loosening and breakage of bonds, etc.; Figure 9), but such models do explain how the expansion or stretching of helically based material can produce twisting with the opposite helical sign.

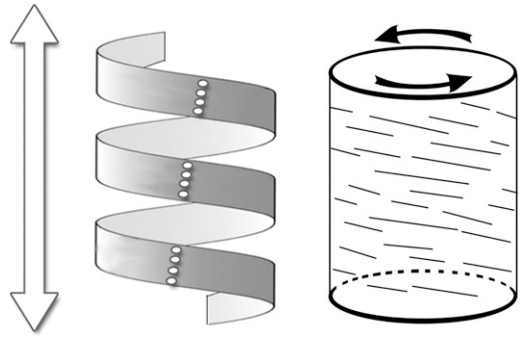

Figure 9. Simple Models Can Explain Helical Growth of Cells Growing in Isolation.

The models link the alignment of structural features with the direction of cell twisting. Arrow on the left indicates the initial direction of expansion. The spring model (center) emphasizes that stretching a left-handed spring can lead to a right-handed displacement of surface landmarks. The model on the right stresses that the load-bearing microfibrils are not interconnected and may reorient during growth. The direction of growth is perpendicular to the mean orientation of microfibrils. This leads to a rotation of the cell's tip relative to its base.

Modeling Shows That Interactions of α-Tubulin with the GTPase Region of β-Tubulin Are Interrupted by the R2K Mutation

If the helicity of the microtubule array and cell twisting can be considered as expressions of microtubule organization, then what impact does the *tor2* amino acid substitution have on this? We showed that the *tor2* phenotype is based on the R2K mutation of α-tubulin 4. The R2 residue of α-tubulin is highly conserved in all eukaryotes. Only a single sequence showing an exchange toward K was found among several hundred GenBank entries. However, the cognate α-tubulin from the planarian *Schmidtea polychroa* is also rather divergent from α-tubulins in other regions of the polypeptide (Simoncelli et al., 2003). The functional importance of the N terminus of α-tubulin was revealed by Ala scanning of the yeast protein (Richards et al., 2000). In *Saccharomyces cerevisiae*, the R2A mutation of α-tubulin (together with an E3A mutation in the same molecule) yielded benomyl supersensitivity and cold sensitivity as well as heat sensitivity. The R2K mutation of α-tubulin described in this article leads to right-handed helical growth in *Arabidopsis* organs and single cells. In a recent publication, Ishida et al. (2007b) presented a set of tubulin mutations leading to helical growth, among those an allele showing the same mutation as *tor2*. They located the mutations to the tubulin heterodimer of a structural model with a maximum resolution of 3.7 Å (Nogales et al., 1999). At 3.7 Å, for structures derived from two-dimensional crystals, the resolution varies considerably in different orientations so that atomic models leave considerable room for interpretation, particularly for the amino acid side chains. Consistently, Ishida et al. did not provide information on hydrogen bonds formed and gave no mechanistic interpretation concerning the effect of the R2K mutation (Ishida et al., 2007b). By contrast, by choosing a structure with 2.89-Å resolution (Nettles et al., 2004), and by confirming the observed interactions through inspection of the respective electron density region, we are able to predict that the wild-type residue R2 of α-tubulin is engaged in an interdimer interaction with Q94 and D74 of β-tubulin via hydrogen bonds. We next modeled the submolecular consequences of the *tor2* amino acid exchange (Figure 1). Results suggest that in the R2K α-tubulin mutant, interdimer interactions are weakened and that intramolecular hydrogen bonds (to T130 and E3 of the same α-tubulin subunit) are favored instead.

The predicted α-tubulin R2 binding partners Q94 and D74 of β-tubulin are located in a region that corresponds to the Switch I and II regions of classical GTPases (Löwe et al., 2001). Switch I and II regions of classical GTPases are involved in GTP binding and hydrolysis (Nogales et al., 1998). It is assumed that the Switch I and II regions of β-tubulin are responsible for the rate of GTP hydrolysis and that this impacts on microtubule dynamic instability (Nogales et al., 1999). Interestingly, in the collection of

tubulin mutants presented by Ishida et al. (2007b), two β-tubulin mutants, S95F and G96D, are reported to show right-handed growth. Indeed, both residues are part of the Switch II region and are located next to Q94, which our models predict to interact with the R2 residue of α-tubulin (Figure 1). This suggests that the region Q94 to G96 of β-tubulin is a hotspot for mutations leading to right-handed growth and supports the idea that this region is important for GTP hydrolysis and normal dynamic instability. Taken together, the results suggest that the R2K mutation exerts its pivotal effect by changing the rate of GTP hydrolysis and thereby microtubule dynamic instability.

It is interesting that the R2K mutation has only been described for the α-tubulin 4 isotype but not for the other α-tubulin genes present in the *Arabidopsis* genome. Although this might indicate a specific function for α-tubulin 4, it seems likely that our screen and the screens by others (Thitamadee et al., 2002; Ishida et al., 2007b) were not at a saturating level to reveal this specific mutation in other α-tubulin isotypes.

The R2K Mutation and Its Effect on Microtubule Dynamics

Because the *tor2* mutation was predicted to impact on microtubule dynamic instability, we analyzed the effect of microtubule drugs on *tor2* root elongation. We found that *tor2* root elongation was hypersensitive to depolymerizing drugs oryzalin and propyzamide. This suggests that microtubules in *tor2* are destabilized. However, we found that *tor2* root elongation was also hypersensitive to the microtubule-stabilizing drug taxol (Figure 3). This argues that the *tor2* defect is not caused by microtubule stabilization or destabilization per se but possibly through a more subtle effect on microtubule behavior. We next asked whether *tor2* is hypersensitive to cold. The effect of cold was studied during hypocotyl etiolation growth, as the phenotypically similar *spr1*/*sku6* mutants respond strong to this procedure (Furutani et al., 2000; Sedbrook et al., 2004). However, we could not observe an obvious enhancement of the *tor2* phenotype in the cold (data not shown). Right-handed growth similar to *tor2* has been observed in plants expressing N-terminally tagged versions of α-tubulin and in an α-tubulin 5 mutant carrying a point mutation and was speculated to be the result of microtubule stabilization. Measuring several parameters of microtubule dynamics prompted those authors to speculate that microtubules in these right-handed mutants are stabilized. It appears that microtubule stability based on drug application was not quantitatively assessed in the case of these mutants (Abe and Hashimoto, 2005; Ishida et al., 2007b). In this regard, it is interesting that the application of the microtubule-stabilizing drug taxol does not produce right-handed, but left-handed growth (Furutani et al., 2000). Taken together, the results for *tor2* do not strictly support a role for microtubule stabilization in contrast with destabilization; rather, they indicate that microtubule stabilization itself is not the driving force behind right-handed helical growth of *tor2*.

To gain better insight into *tor2* microtubule dynamics, we used GFP-tagged EB1 and TUB6 markers and investigated microtubule behavior in detail. This showed that not only was the rate of microtubule polymerization reduced in *tor2*, but the rate of microtubule depolymerization also. As a result, microtubule dynamicity is diminished in *tor2*. Microtubule dynamicity is a measure for the total amount of polymer gained or lost per time. The fact that *tor2* microtubules spent more time in pause would decrease dynamicity further (Figure 2). It is interesting that we find both catastrophe and rescue frequencies increased in *tor2*, and it is possible that this functionally mirrors the increased sensitivity to stabilizing and destabilizing microtubule drugs (Figure 3). Next, we measured the density of microtubules at the cell's cortex but could not find significantly more microtubules or microtubule bundles in cells of *tor2* (see Supplemental Figure 3 online). This differs from what was obtained for an α-tubulin 5 point mutation (Ishida et al., 2007b) and adds support to the idea that microtubules are not simply stabilized in *tor2*. Since EB1 has been suggested to have an affinity for the GTP cap of a microtubule (Tirnauer et al., 2002), which is a measure of continuing microtubule growth, we examined the length of the EB1 comets. Results confirm that EB1 plus end comets in *tor2* plants are larger than those in the wild type (Figure 2G). In conclusion, and as suggested from our structural analysis, the *tor2* mutation of α-tubulin has a strong impact on microtubule dynamic instability, and this is likely the result of interfering with the GTPase function of β-tubulin. The observed reduction in dynamicity may reduce the capacity of the array to reorient in response to external or internal cues.

Putative Mechanisms of Helical Growth

There is a long history of helically based cell walls producing the twisting of filamentous algae (Frei and Preston, 1961; Probine, 1963; Roelofsen, 1965), and this study suggests that the growth pattern of higher plants may be traced back to the behavior of their isolated cells (as seen in trichome cells of *tor2*). As left-handed microtubule arrays are seen very early during trichome development, we suggest that this is the reason for right-handed cell features of mature *tor2* trichomes (Figures 6 and 7). The question then is how are these helical arrays established in the first place?

Plant microtubule arrays are thought to be constructed from the way that treadmilling microtubules (Shaw et al., 2003) interact. Collisions at shallow angles are thought to lead to parallelization of growth, while steeper collisions lead either to catastrophic depolymerization (Dixit and Cyr, 2004) or crossover (Shaw et al., 2003; Wightman and Turner, 2007). Microtubules are born either at random sites at the cortex (Shaw et al., 2003) or branch from foci upon mother microtubules (Murata et al., 2005). Although no obvious asymmetries have so far been described at this level of plant microtubule behavior, at a larger scale microtubules have been reported to produce uniform tissue fields with a common helical sign in wild-type *Arabidopsis* and maize (*Zea mays*; Liang et al., 1996). It seems possible that helical growth as described for *tor2* has its origin in such naturally occurring microtubule array asymmetries but under circumstances where growth and microtubule reorientation become desynchronized. In roots, for example, helical arrays develop only at the end of the cell elongation phase (Liang et al., 1996; Sugimoto et al., 2000). These handed arrays may have little effect on wild-type organ shape (however, see Simmons et al., 1995), but it is conceivable that in, for example, left-handed helical growth mutants, this reorientation to right-handed helical arrays occurs prematurely,

thereby causing helical organ growth. Likewise, it seems possible that a change in microtubule dynamicity observed in *tor2* impacts on microtubule reorientations, desynchronizing growth and microtubule positioning.

In conclusion, the results presented here show that the R2K mutation of α-tubulin leads to right-handed helical growth of organs and isolated cells. Our high-resolution analysis of the tubulin structure shows that the R2 residue of α-tubulin interacts through hydrogen bonds with the GTPase Switch regions of β-tubulin and that these interactions are not formed by the mutant tubulin. These results suggest that the *tor2* phenotype is likely to result from an effect on microtubule dynamic instability. Indeed, testing several parameters of microtubule dynamics in living *Arabidopsis* cells clearly reveals an effect on microtubule behavior. We next used the *tor2* mutant to investigate the developmental origin of helical growth. Because the application of the antimicrotubule drug propyzamide allows the manipulation of the twisting direction in nondividing hypocotyls, we reject the hypothesis that organ twisting is based on cell division patterns. Moreover, *tor2* is the first *Arabidopsis* mutant reported to show helical growth in isolated cells. We show that mature trichomes of *tor2* have a consistent right-handed twist, and this is preceded by the formation of left-handed cortical microtubule arrays in developing trichomes. According to these observations, we hypothesize that in *tor2*, the twisting of individual cells directly translates into the higher-order twisting of organs.

METHODS

Mutant Strains and Mutation Mapping

Mutants displaying the *tor* phenotype were identified in an ethane methylsulfonate–mutagenized *Arabidopsis thaliana* L*er* population. Allelism tests revealed several complementation groups. The *tor2* mutation is inherited as a semidominant trait. Additional genetic markers for chromosome 1 facilitated the identification of *tor2*. New markers were developed using the method of DNA duplex analysis (Hauser et al., 1998).

Double mutants with *tor2* were identified in F2 populations generated by crossings to the respective mutant lines. The double homozygous situation was verified by PCR (flanking markers, deletions) or by outcrossing into the wild type (*zwichel* 9311-11 mutant). The *zwichel* 9311-11 mutant was kindly provided by David Oppenheimer. A homozygous knockout α-tubulin 4 mutant (SALK_080530) was identified in the SALK collection (Alonso et al., 2003), and the absence of the corresponding transcript in the mutant was confirmed by RT-PCR in comparison to PCR from wild-type cDNA (see Supplemental Figure 1 online).

Transgenic Approaches

Genomic constructs encompassing wild-type TUA4 or mutant *tua4*^{K2R} genes were polymerized by PCR using forward primer 5′-GGGGACAAGTTTGTACAAAAAAGCAGGCTAAATTCCAATGATCCCCTCA-3′ and reverse primer 5′-GGGGACCACTTTGTACAAGAAAGCTGGGTGCTATATCCTCACTGCCACA-3′ based on AGI gene predictions, cloned into GATEWAY vector pDONR221 (Invitrogen), and verified by DNA sequencing. Obtained entry vectors were recombined with destination vectors pKGW and pBGW to generate plant expression constructs (Karimi et al., 2002).

Transgenic L*er* lines expressing EB1-GFP were generated by transforming L*er* wild-type plants with a $35S_{pro}$:EB1-GFP construct (Chan et al., 2003). Obtained lines were crossed to the homozygous *tor2* mutant and control, and *tor2* lines were bred from progeny of such crosses. Transgenic lines expressing a GFP-TUB6 fusion were obtained by transforming *tor2* and L*er* plants with pBGW-$35S_{pro}$:sGFP-TUB6. For this construct, three fragments encompassing the cauliflower mosaic virus $35S_{pro}$:synthetic GFP sequence (Chiu et al., 1996), the *Arabidopsis* TUB6 open reading frame, and the nopaline synthase terminator were fused by a PCR strategy and subsequently recombined into pBGW (Karimi et al., 2002). The construct allows the constitutive expression of sGFP with C-terminally linked full-length TUB6. The linker between sGFP and TUB6 is ala-gly-ala-gly. All plant transformations were performed by floral dip (Clough and Bent, 1998).

Structural Analyses

Structural models and structure factors were downloaded from Protein Data Bank (www.rcsb.org). All detailed analyses were based on structural information with the highest available resolution (Nettles et al., 2004; PDB-ID: 1TVK; resolution of 2.89 Å). We used the program Coot (Emsley and Cowtan, 2004) to perform symmetry operations for the generation of complete structural models. Structure factors were converted into MTZ files using the CCP4 program suite (Collaborative Computational Project, 1994) and analyzed with Coot. The R2K mutation was generated in Coot and optimized using standard rotamer library. Images were generated with Pymol (DeLano Scientific).

Drug Treatments

For the analysis of root elongation and hypocotyl twisting, plants were germinated on MS-based media containing the indicated drug concentration. Stocks of microtubule drugs (Sigma-Aldrich) were prepared in DMSO. Experiments to generate taxol-induced trichome branching were based on a procedure described elsewhere (Mathur and Chua, 2000).

Cell Suspensions

tor2 and L*er* callus cultures were generated from root cuttings by placing them on agar medium as described earlier (May and Leaver, 1993). After sufficient callus growth (2 to 3 weeks) cells were transferred to fresh plates and eventually into liquid MS medium supplemented with 2,4-D. Obtained suspension lines were subbed weekly.

Confocal Microscopy, Analysis of Image Data, and Microtubule Dynamics

Propidium iodide–based microscopy of roots was performed on living specimens using the Leica SP2 confocal microscope. Sufficient staining was achieved using 100 μg/mL propidium iodide (Sigma-Aldrich) in diluted MS medium for 30 min. GFP-based microscopy of trichomes and roots and for the analysis of microtubule dynamics was performed using the Visitech spinning disc confocal microscope using a 60-fold immersion objective. Data were collected using Metamorph software. Movies were assembled and analyzed with the help of the ImageJ software (W. Rasband, National Institutes of Health).

Movies for the analysis of microtubule dynamics were based on 61 projections from four z-sections acquired every 4 s (4 min total length; measured at 24°C). As a rule of thumb, microtubules were randomly selected in stills, and their behavior was then followed in the respective movies. Rate of polymerization and depolymerization was measured from kymographs. This involved the plugin Multiple Kymograph and the macro Read Velocities from Tsp (J. Rietdorf, EMBL, Heidelberg, Germany). EB1 comet profiles were measured using the Plot Profile function of ImageJ. Catastrophe and rescue frequencies were calculated in relation to total time spent because catastrophe and rescue were often observed to occur out of the paused state (especially in *tor2*). This was based on

randomly selected microtubules regardless of their previous life history. This seemed appropriate since in plant cortical arrays the origin of microtubules is often beyond the area of observation and polymerization can occur for longer than the time frame of observation (see Figure 2F). These microtubules would otherwise escape the measurement. For a somewhat different approximation, see Cassimeris et al. (1988). For statistical analyses, data were checked for normality and F-tests and *t* tests were performed using Microsoft Excel.

Scanning Electron Microscopy

Leaf samples (fourth or fifth true leaf) were mounted on an aluminum stub using O.C.T. compound (BDH Laboratory Supplies). The stub was then immediately plunged into liquid nitrogen slush to cryopreserve the material. The sample was transferred onto the cryostage of an ALTO 2500 cryo-transfer system (Gatan) attached to a Zeiss Supra 55 VP FEG scanning electron microscope. Sublimation of surface frost was performed at −95°C for 3 min before sputter coating the sample with platinum for 2 min at 10 mA, at temperatures below −110°C. After sputter coating, the sample was moved onto the cryostage in the main chamber of the microscope and held at approximately −130°C. The sample was imaged at 3 kV, and digital TIFF files were stored.

Accession Numbers

Sequence data from this article can be found in the Arabidopsis Genome Initiative or GenBank/EMBL databases under the following accession numbers: *TUB9* (At4g20890), *EB1* (At3g47690), and sGFP (EF090408). *tor2* mutants carry a point mutation in the α-tubulin 4 gene of *Arabidopsis* (Arabidopsis Genome Initiative number At1g04820).

Author Contributions

H.B., C.W.L., and A.R.S. designed the research. H.B., M.H., D.N., and A.R.S. performed the research. H.B., C.W.L., D.N., and A.R.S. analyzed the data. H.B. wrote the article, and C.W.L., D.N., and A.R.S. contributed to the writing.

Supplemental Data

The following materials are available in the online version of this article.

Supplemental Figure 1. RT-PCR Verification of *tua4* Knockout Line.

Supplemental Figure 2. Modeling of Intramolecular Interactions of Mutant α-Tubulin K2.

Supplemental Figure 3. Microtubule Density of *tor2* Is Similar to That of the Wild Type.

Supplemental Figure 4. Direct Comparison of EB1-GFP Comets Seen in Hypocotyl Cells of *tor2* and the Wild-Type.

Supplemental Figure 5. Additional *tor2* Phenotypes.

Supplemental Figure 6. Quantitative Analysis of the Dwarf Phenotype Caused by the *tor2* Mutation and Effects on the Growth Anisotropy of Epidermal Cells.

Supplemental Figure 7. Ploidy Levels in Leaves of *tor2* Are Similar to the Wild Type.

Supplemental Figure 8. Left-Handed *tortifolia3* Mutant.

Supplemental Movie 1. Microtubule Dynamics in 3-d-Old Cotyledon Epidermal Cells Expressing GFP-TUB6.

Supplemental Movie 2. Wild-Type Trichomes before Branching Expressing EB1-GFP.

Supplemental Movie 3. *tor2* Trichome before Branching Expressing EB1-GFP.

ACKNOWLEDGMENTS

We thank Kim Findlay for advice and help with the scanning electron microscope, John Doonan and Max Bush for help with the flow cytometer, Grant Calder and Adrian Sambade for suggestions concerning the study of microtubule dynamics, and Christoph Fabri for the initial morphological characterization of *tor2*. Birgit Geist provided excellent technical assistance. This work was supported by the Deutsche Forschungsgemeinschaft (Scha 454/5, Ni 1110/1-1), by Fonds der Chemischen Industrie, the President's Fund of the Helmholtz Association (VH-NG 142), and by a Biotechnology and Biological Science Research Council grant to C.W.L.

Received June 9, 2008; revised June 17, 2009; accepted July 10, 2009; published July 28, 2009.

REFERENCES

Abe, T., and Hashimoto, T. (2005). Altered microtubule dynamics by expression of modified alpha-tubulin protein causes right-handed helical growth in transgenic *Arabidopsis* plants. Plant J. **43:** 191–204.

Alonso, J.M., et al. (2003). Genome-wide insertional mutagenesis of *Arabidopsis thaliana.* Science **301:** 653–657.

Anders, K.R., and Botstein, D. (2001). Dominant-lethal alpha-tubulin mutants defective in microtubule depolymerization in yeast. Mol. Biol. Cell **12:** 3973–3986.

Anthony, R.G., Waldin, T.R., Ray, J.A., Bright, S.W., and Hussey, P.J. (1998). Herbicide resistance caused by spontaneous mutation of the cytoskeletal protein tubulin. Nature **393:** 260–263.

Baskin, T.I. (2001). On the alignment of cellulose microfibrils by cortical microtubules: A review and a model. Protoplasma **215:** 150–171.

Baskin, T.I. (2005). Anisotropic expansion of the plant cell wall. Annu. Rev. Cell Dev. Biol. **21:** 203–222.

Baum, S.F., and Rost, T.L. (1996). Root apical organization in *Arabidopsis thaliana*. 1. Root cap and protoderm. Protoplasma **192:** 178–188.

Buey, R.M., Diaz, J.F., and Andreu, J.M. (2006). The nucleotide switch of tubulin and microtubule assembly: A polymerization-driven structural change. Biochemistry **45:** 5933–5938.

Buschmann, H., Fabri, C.O., Hauptmann, M., Hutzler, P., Laux, T., Lloyd, C.W., and Schäffner, A.R. (2004). Helical growth of the *Arabidopsis* mutant *tortifolia1* reveals a plant-specific microtubule-associated protein. Curr. Biol. **14:** 1515–1521.

Buschmann, H., and Lloyd, C.W. (2008). *Arabidopsis* mutants and the network of microtubule-associated functions. Mol. Plant **1:** 888–898.

Cassimeris, L., Pryer, N.K., and Salmon, E.D. (1988). Real-time observations of microtubule dynamic instability in living cells. J. Cell Biol. **107:** 2223–2231.

Chan, J., Calder, G.M., Doonan, J.H., and Lloyd, C.W. (2003). EB1 reveals mobile microtubule nucleation sites in *Arabidopsis.* Nat. Cell Biol. **5:** 967–971.

Chiu, W., Niwa, Y., Zeng, W., Hirano, T., Kobayashi, H., and Sheen, J. (1996). Engineered GFP as a vital reporter in plants. Curr. Biol. **6:** 325–330.

Clough, S.J., and Bent, A.F. (1998). Floral dip: A simplified method for *Agrobacterium*-mediated transformation of *Arabidopsis thaliana.* Plant J. **16:** 735–743.

Cnops, G., Wang, X., Linstead, P., Van Montagu, M., Van Lijsebettens, M., and Dolan, L. (2000). Tornado1 and tornado2 are required for the specification of radial and circumferential pattern in the *Arabidopsis* root. Development **127:** 3385–3394.

Collaborative Computational Project, Number 4 (1994). The CCP4 suite: programs for protein crystallography. Acta Crystallogr. D Biol. Crystallogr. **50:** 760–763.

Collett, C.E., Harberd, N.P., and Leyser, O. (2000). Hormonal interactions in the control of *Arabidopsis* hypocotyl elongation. Plant Physiol. **124:** 553–562.

Dixit, R., and Cyr, R. (2004). Encounters between dynamic cortical microtubules promote ordering of the cortical array through angle-dependent modifications of microtubule behavior. Plant Cell **16:** 3274–3284.

Emsley, P., and Cowtan, K. (2004). Coot: Model-building tools for molecular graphics. Acta Crystallogr. D Biol. Crystallogr. **60:** 2126–2132.

Fabri, C.O., and Schäffner, A.R. (1994). An *Arabidopsis thaliana* RFLP mapping set to localize mutations to chromosome regions. Plant J. **5:** 149–156.

Feenstra, W.J. (1978). Contiguity of linkage groups I and IV as revealed by linkage relationship of two newly isolated markers *dis-1* and *dis-2.* Arabidopsis Inf. Serv. **15:** 35–38.

Frei, E., and Preston, R.D. (1961). Cell wall organization and wall growth in the filamentous green algae *Cladophora* and *Chaetomorpha* II. Proc. R. Soc. Lond. B. Biol. Sci. **155:** 55–77.

Furutani, I., Watanabe, Y., Prieto, R., Masukawa, M., Suzuki, K., Naoi, K., Thitamadee, S., Shikanai, T., and Hashimoto, T. (2000). The SPIRAL genes are required for directional control of cell elongation in *Arabidopsis thaliana.* Development **127:** 4443–4453.

Gendreau, E., Traas, J., Desnos, T., Grandjean, O., Caboche, M., and Höfte, H. (1997). Cellular basis of hypocotyl growth in *Arabidopsis thaliana.* Plant Physiol. **114:** 295–305.

Hashimoto, T. (2002). Molecular genetic analysis of left-right handedness in plants. Philos. Trans. R. Soc. Lond. B Biol. Sci. **357:** 799–808.

Hauser, M.T., Adhami, F., Dorner, M., Fuchs, E., and Glossl, J. (1998). Generation of co-dominant PCR-based markers by duplex analysis on high resolution gels. Plant J. **16:** 117–125.

Hülskamp, M., Misra, S., and Jürgens, G. (1994). Genetic dissection of trichome cell development in *Arabidopsis.* Cell **76:** 555–566.

Ishida, T., Kaneko, Y., Iwano, M., and Hashimoto, T. (2007b). Helical microtubule arrays in a collection of twisting tubulin mutants of *Arabidopsis thaliana.* Proc. Natl. Acad. Sci. USA **104:** 8544–8549.

Ishida, T., Thitamadee, S., and Hashimoto, T. (2007a). Twisted growth and organization of cortical microtubules. J. Plant Res. **120:** 61–70.

Jürgens, G. (2005). Cytokinesis in higher plants. Annu. Rev. Plant Biol. **56:** 281–299.

Kaloriti, D., Galva, C., Parupalli, C., Khalifa, N., Galvin, M., and Sedbrook, J.C. (2007). Microtubule associated proteins in plants and the processes they manage. J. Integr. Plant Biol. **49:** 1164–1173.

Karimi, M., Inze, D., and Depicker, A. (2002). GATEWAY vectors for *Agrobacterium*-mediated plant transformation. Trends Plant Sci. **7:** 193–195.

Liang, B.M., Dennings, A.M., Sharp, R.E., and Baskin, T.I. (1996). Consistent handedness of microtubule arrays in maize and *Arabidopsis* primary roots. Protoplasma **190:** 8–15.

Lloyd, C., and Buschmann, H. (2007). Plant division: Remembering where to build the wall. Curr. Biol. **17:** 1053–1055.

Lloyd, C., and Chan, J. (2002). Helical microtubule arrays and spiral growth. Plant Cell **14:** 2319–2324.

Löwe, J., Li, H., Downing, K.H., and Nogales, E. (2001). Refined structure of alpha beta-tubulin at 3.5 Å resolution. J. Mol. Biol. **313:** 1045–1057.

Luo, D., and Oppenheimer, D.G. (1999). Genetic control of trichome branch number in *Arabidopsis*: The roles of the FURCA loci. Development **126:** 5547–5557.

Mathur, J., and Chua, N.H. (2000). Microtubule stabilization leads to growth reorientation in *Arabidopsis* trichomes. Plant Cell **12:** 465–477.

May, M.J., and Leaver, C.J. (1993). Oxidative stimulation of glutathione synthesis in *Arabidopsis thaliana* suspension cultures. Plant Physiol. **103:** 621–627.

McKean, P.G., Vaughan, S., and Gull, K. (2001). The extended tubulin superfamily. J. Cell Sci. **114:** 2723–2733.

Morrissette, N.S., Mitra, A., Sept, D., and Sibley, L.D. (2004). Dinitroanilines bind alpha-tubulin to disrupt microtubules. Mol. Biol. Cell **15:** 1960–1968.

Müller, S., Wright, A.J., and Smith, L.G. (2009). Division plane control in plants: new players in the band. Trends Cell Biol. **19:** 180–188.

Murata, T., Sonobe, S., Baskin, T.I., Hyodo, S., Hasezawa, S., Nagata, T., Horio, T., and Hasebe, M. (2005). Microtubule-dependent microtubule nucleation based on recruitment of gamma-tubulin in higher plants. Nat. Cell Biol. **7:** 961–968.

Nakajima, K., Furutani, I., Tachimoto, H., Matsubara, H., and Hashimoto, T. (2004). SPIRAL1 encodes a plant-specific microtubule-localized protein required for directional control of rapidly expanding *Arabidopsis* cells. Plant Cell **16:** 1178–1190.

Nakamura, M., and Hashimoto, T. (2009). A mutation in the *Arabidopsis* γ-tubulin-containing complex causes helical growth and abnormal microtubule branching. J. Cell Sci. **122:** 2208–2217.

Nettles, J.H., Li, H., Cornett, B., Krahn, J.M., Snyder, J.P., and Downing, K.H. (2004). The binding mode of epothilone A on alpha, beta-tubulin by electron crystallography. Science **305:** 866–869.

Nogales, E., Downing, K.H., Amos, L.A., and Lowe, J. (1998). Tubulin and FtsZ form a distinct family of GTPases. Nat. Struct. Biol. **5:** 451–458.

Nogales, E., Whittaker, M., Milligan, R.A., and Downing, K.H. (1999). High-resolution model of the microtubule. Cell **96:** 79–88.

Oppenheimer, D.G., Pollock, M.A., Vacik, J., Szymanski, D.B., Ericson, B., Feldmann, K., and Marks, M.D. (1997). Essential role of a kinesin-like protein in *Arabidopsis* trichome morphogenesis. Proc. Natl. Acad. Sci. USA **94:** 6261–6266.

Paredez, A., Somerville, C., and Ehrhardt, D. (2006). Visualization of cellulose synthase demonstrates functional association with microtubules. Science **312:** 1491–1495.

Perrin, R.M., Wang, Y., Yuen, C.Y., Will, J., and Masson, P.H. (2007). WVD2 is a novel microtubule-associated protein in *Arabidopsis thaliana.* Plant J. **49:** 961–971.

Pfosser, M., Magyar, Z., and Bögre, L. (2007). Cell cycle analysis in plants. In Flow Cytometry with Plant Cells: Analysis of Genes, Chromosomes and Genomes, J. Doležel, J. Greilhuber, and J. Suda, eds (Wiley-VCH Verlag, Weinhem), pp. 323–347.

Preston, R.D. (1974). The Physical Biology of Plant Cell Walls. (London: Chapman & Hall).

Probine, M.C. (1963). Cell growth and the structure and mechanical properties of the wall in internodal cells of *Nitella opaca*. III. Spiral growth and cell wall structure. J. Exp. Bot. **14:** 101–113.

Reddy, A.S., and Day, I.S. (2000). The role of the cytoskeleton and a molecular motor in trichome morphogenesis. Trends Plant Sci. **5:** 503–505.

Reinholz, E. (1947). Auslösung von Röntgen-Mutationen bei *Arabidopsis thaliana* (L.) HEYNH. und ihre Bedeutung für die Pflanzenzüchtung und Evolutionstheorie. FIAT Report **1006:** 1–70.

Richards, K.L., Anders, K.R., Nogales, E., Schwartz, K., Downing, K.H., and Botstein, D. (2000). Structure-function relationships in yeast tubulins. Mol. Biol. Cell **11:** 1887–1903.

Roelofsen, P.A. (1950). Cell-wall structure in the growth-zone of *Phycomyces* sporangiophores. I. Model experiments and microscopical observations. Biochim. Biophys. Acta **6:** 340–356.

Roelofsen, P.A. (1951). Cell-wall structure in the growth-zone of *Phycomyces* sporangiophores. II. Double refraction and electron microscopy. Biochim. Biophys. Acta **6:** 357–373.

Roelofsen, P.A. (1965). Ultrastructure of the wall in growing cells and its relation to the direction of growth. Adv. Bot. Res. **2:** 69–149.

Saedler, R., Mathur, N., Srinivas, B.P., Kernebeck, B., Hulskamp, M., and Mathur, J. (2004). Actin control over microtubules suggested by DISTORTED2 encoding the Arabidopsis ARPC2 subunit homolog. Plant Cell Physiol. **45:** 813–822.

Sedbrook, J.C. (2004). MAPs in plant cells: Delineating microtubule growth dynamics and organization. Curr. Opin. Plant Biol. **7:** 632–640.

Sedbrook, J.C., Ehrhardt, D.W., Fisher, S.E., Scheible, W.R., and Somerville, C.R. (2004). The *Arabidopsis* SKU6/SPIRAL1 gene encodes a plus end-localized microtubule-interacting protein involved in directional cell expansion. Plant Cell **16:** 1506–1520.

Shaw, S.L., Kamyar, R., and Ehrhardt, D.W. (2003). Sustained microtubule treadmilling in Arabidopsis cortical arrays. Science **300:** 1715–1718.

Shoji, T., Narita, N.N., Hayashi, K., Asada, J., Hamada, T., Sonobe, S., Nakajima, K., and Hashimoto, T. (2004). Plant-specific microtubule-associated protein SPIRAL2 is required for anisotropic growth in *Arabidopsis.* Plant Physiol. **136:** 3933–3944.

Simmons, C., Söll, D., and Miglicaccio, F. (1995). Circumnutation and gravitropism cause root waving in *Arabidopsis thaliana.* J. Exp. Bot. **46:** 143–150.

Simoncelli, F., Sorbolini, S., Fagotti, A., Di Rosa, I., Porceddu, A., and Pascolini, R. (2003). Molecular characterization and expression of a divergent alpha-tubulin in planarian *Schmidtea polychroa.* Biochim. Biophys. Acta **1629:** 26–33.

Sugimoto, K., Himmelspach, R., Williamson, R.E., and Wasteneys, G.O. (2003). Mutation or drug-dependent microtubule disruption causes radial swelling without altering parallel cellulose microfibril deposition in *Arabidopsis* root cells. Plant Cell **15:** 1414–1429.

Sugimoto, K., Williamson, R.E., and Wasteneys, G.O. (2000). New techniques enable comparative analysis of microtubule orientation, wall texture, and growth rate in intact roots of *Arabidopsis.* Plant Physiol. **124:** 1493–1506.

Szymanski, D.B., Marks, M.D., and Wick, S.M. (1999). Organized F-actin is essential for normal trichome morphogenesis in *Arabidopsis*. Plant Cell **11:** 2331–2347.

Thitamadee, S., Tuchihara, K., and Hashimoto, T. (2002). Microtubule basis for left-handed helical growth in *Arabidopsis.* Nature **417:** 193–196.

Tirnauer, J.S., Grego, S., Salmon, E.D., and Mitchison, T.J. (2002). EB1-microtubule interactions in Xenopus egg extracts: Role of EB1 in microtubule stabilization and mechanisms of targeting to microtubules. Mol. Biol. Cell **13:** 3614–3626.

Wasteneys, G.O., and Collings, D.A. (2004). Expanding beyond the great divide: The cytoskeleton and axial growth. In The Plant Cytoskeleton in Cell Differentiation and Development, P.J. Hussey, ed (Oxford: Blackwell Publishing, CRC Press), pp. 83–115.

Whittington, A.T., Vugrek, O., Wei, K.J., Hasenbein, N.G., Sugimoto, K., Rashbrooke, M.C., and Wasteneys, G.O. (2001). MOR1 is essential for organizing cortical microtubules in plants. Nature **411:** 610–613.

Wightman, R., and Turner, S.R. (2007). Severing at sites of microtubule crossover contributes to microtubule alignment in cortical arrays. Plant J. **52:** 742–751.

Yuen, C.Y., Pearlman, R.S., Silo-Suh, L., Hilson, P., Carroll, K.L., and Masson, P.H. (2003). WVD2 and WDL1 modulate helical organ growth and anisotropic cell expansion in *Arabidopsis.* Plant Physiol. **131:** 493–506.

Zhang, X., Dyachok, J., Krishnakumar, S., Smith, L.G., and Oppenheimer, D.G. (2005). IRREGULAR TRICHOME BRANCH1 in Arabidopsis encodes a plant homolog of the actin-related protein2/3 complex activator Scar/WAVE that regulates actin and microtubule organization. Plant Cell **17:** 2314–2326.